

Magnetic breakdown and Klein tunneling in a type-II Weyl semimetal

T. E. O'Brien, M. Diez, and C. W. J. Beenakker

Instituut-Lorentz, Universiteit Leiden, P.O. Box 9506, 2300 RA Leiden, The Netherlands

(Dated: April 2016)

The band structure of a type-II Weyl semimetal has pairs of electron and hole pockets that coexist over a range of energies and touch at a topologically protected conical point. We identify signatures of this Weyl point in the magnetic quantum oscillations of the density of states, observable in thermodynamic properties. Tunneling between the electron and hole pockets in a magnetic field is the momentum space counterpart of Klein tunneling at a p - n junction in real space. This magnetic breakdown happens at a characteristic field that vanishes when the Fermi level approaches the Weyl point, and is signaled by the suppression of high-frequency components of the magnetic oscillations.

Weyl semimetals provide a condensed matter realization of massless relativistic fermions [1]. Their spectrum features a diabolical surface in energy-momentum space that separates helical electron-like states (moving in the direction of the momentum) from hole-like states (moving opposite to the momentum) [2]. These “Weyl cones” are the three-dimensional analogue of the two-dimensional Dirac cones in graphene. The third spatial dimension provides a topological protection, by which the conical point (Weyl point) cannot be opened up unless two Weyl cones of opposite helicity are brought together in momentum space [3].

Although the Weyl point cannot be locally removed, the cones can be tilted and may even tip over [4–8]. For the relativistic Weyl cone such a distortion is forbidden by particle-hole symmetry, but that is not a fundamental symmetry in condensed matter. While in graphene the high symmetry of the honeycomb lattice keeps the cone upright, strain providing only a weak tilt [9], the tilting can be strong in 3D Weyl semimetals. This leads to a natural division of Weyl cones into two topologically distinct types [6]. In type I, the cone is only weakly tilted so that the electron-like states and hole-like states occupy separate energy ranges, above or below the Weyl point. In type II the cone has tipped over so that electron and hole states coexist in energy. Experimental realizations of a type-II Weyl semimetal have recently been reported [10–12].

In a magnetic field the coexisting electron and hole pockets of a type-II Weyl semimetal are coupled by tunneling through the Weyl point. Here we investigate how this process, a momentum space manifestation of Klein tunneling [13], affects the magnetic quantum oscillations of the density of states (De Haas-Van Alphen effect), providing a unique thermodynamic signature of the topologically protected band structure (an alternative to proposed transport signatures [6, 14, 15]). Because the quantum oscillations are governed by extremal cross-sections of the Fermi surface, one might wonder whether some high symmetry is required to align the extremal cross-section with the Weyl point, so that it becomes observable. Our analysis shows that a magnetic field axis for this alignment exists generically, because of the Möbius strip topology of the projective plane.

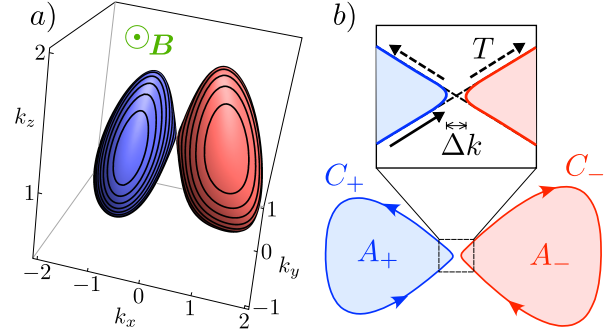


FIG. 1: a) Fermi surface of a type-II Weyl semimetal, calculated from the model Hamiltonian (1), showing the electron and hole pockets touching at the Weyl point. Equi-energy contours in a plane perpendicular to the magnetic field B are indicated. The magnetic quantum oscillations have a periodicity in $1/B$ determined by the contour that encloses an extremal area. b) Intersection of the Fermi surface with a plane perpendicular to B that passes through the Weyl point. Electron and hole pockets are bounded by a contour C_{\pm} enclosing an area A_{\pm} . The semiclassical orbit of an electron follows the contour in the direction of the arrow. Tunneling between the pockets happens with a probability T that tends to unity when their minimal separation $\Delta k \rightarrow 0$. This magnetic breakdown is a manifestation of Klein tunneling in momentum space.

To first order in momentum \mathbf{k} , the Hamiltonian of a Weyl cone has the generic form

$$H = \sum_{ij} v_{ij} k_i k_j + a_{\text{tilt}} k_x \sigma_0, \quad (1)$$

in terms of Pauli matrices σ_i , $i \in \{x, y, z\}$ (unit matrix σ_0). The eigenvalues lie on two hyperboloid sheets E_{\pm} ,

$$E_{\pm} = a_{\text{tilt}} k_x \pm \sqrt{\sum_{ijl} v_{il} v_{jl} k_i k_j}, \quad (2)$$

that touch at the Weyl point $\mathbf{k} = 0$.

For sufficiently small a_{tilt} , the Fermi surface contains either electron-like states in E_+ or hole-like states in E_- , depending on the sign of the Fermi energy. With increasing a_{tilt} the Weyl cone is tilted in the (arbitrarily chosen) x -direction, and when it tips over coexisting electron and hole states appear on the Fermi surface. This is the type-I to type-II Weyl semimetal transition [6].

The hyperboloid dispersion (2) only holds near the Weyl point. In the proposed [6, 11] physical realizations of a type-II Weyl semimetal the Fermi surface closes away from the Weyl point, forming compact electron and hole pockets. A cross-section is defined by fixing an axis (unit vector \hat{n}) and choosing a coordinate q along that axis. The intersection of the Fermi surface with the plane $\hat{n} \cdot \mathbf{k} = q$ is an oriented contour $C_{\pm}(q)$ enclosing the signed area $A_{\pm}(q)$ (positive for C_+ and negative for C_-). The contours are the classical momentum-space orbits for a magnetic field B in the \hat{n} -direction, the change in orientation between C_+ and C_- resulting from the sign change of the effective mass in the electron and hole pockets.

Semiclassical quantization of the orbits produces Landau tubes [16], with quantized cross-sectional area

$$A_{\pm}(q) = 2\pi n e B / \hbar, \quad n = \pm 1, \pm 2, \dots \quad (3)$$

These give rise to oscillations in the density of states periodic in $1/B$, with frequency given by the Onsager relation [17, 18]

$$F_{\pm} \equiv \frac{1}{\Delta(1/B)} = \frac{\hbar}{2\pi e} |A_{\pm}|. \quad (4)$$

The extremal area A_{\pm} is the area at which $dA_{\pm}(q)/dq = 0$. The contour enclosing the extremal area is denoted by C_{\pm} .

The two sheets E_{\pm} of a type-II Weyl cone are coupled by quantum tunneling. This magnetic-field-induced tunneling between electron and hole pockets is the momentum space counterpart of Klein tunneling at a p - n junction in graphene [19], and can be analyzed along the same lines [20].

The effect of a magnetic field B in, say, the y -direction, with vector potential $\mathbf{A} = (Bz, 0, 0)$, is accounted for by the substitution $k_x \mapsto k_x + eBz$ (setting $\hbar = 1$). In momentum representation, the Schrödinger equation $H\psi = E\psi$ reads

$$iU_0 \frac{\partial \psi}{\partial k_z} = U(k_z)\psi, \quad U_0 = eB(\sum_j v_{xj}\sigma_j + a_{\text{tilt}}\sigma_0), \quad (5a)$$

$$U(k_z) = E\sigma_0 - \sum_{ij} v_{ij}k_i\sigma_j - a_{\text{tilt}}k_x\sigma_0. \quad (5b)$$

For $a_{\text{tilt}} > (\sum_j v_{xj}^2)^{1/2}$ the matrix U_0 is positive definite, so that it can be factorized as $U_0 = VV^{\dagger}$ with invertible V and we may write

$$i \frac{\partial \psi}{\partial k_z} = V^{-1}U(k_z)(V^{\dagger})^{-1}\psi \equiv \mathcal{H}(k_z)\psi, \quad (6)$$

$$\mathcal{H}(k_z) = \mathcal{H}_0 + \mathcal{H}_1 k_z.$$

If we interpret $k_z \equiv t$ as “time”, this looks like a Schrödinger equation for a spin-1/2 particle with “time”-dependent Hamiltonian $\mathcal{H}(t)$. Because the t -dependence of $\mathcal{H}(t)$ is linear, we can use the Landau-Zener formula for the tunneling probability between the electron and hole pockets [21].

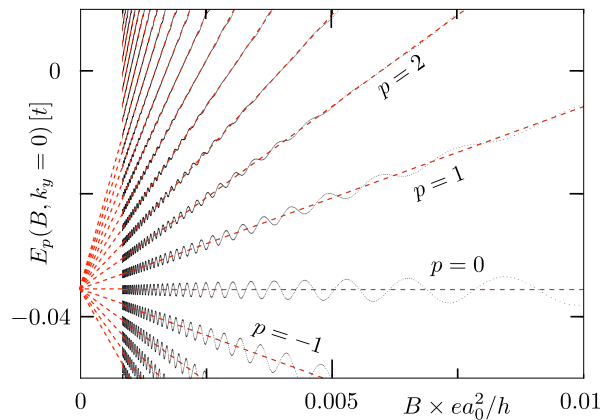


FIG. 2: Energy spectrum at $k_y = 0$ of the type-II Weyl semimetal with Hamiltonian (10) (parameters $t = 1$, $t' = 2$, $\mu = 3$, $b = 1.2$, $a_{\text{tilt}} = 1.7$, $\xi = 0.08$). The black dotted curves are the exact numerical results, the red dashed lines form the semiclassical Landau fan (14) for tunnel-coupled electron and hole pockets. The individual pockets are responsible for the high-frequency oscillations superimposed on the fan.

Quite generally, for a two-level system with time-dependent Hamiltonian

$$\mathcal{H}(t) = \begin{pmatrix} \alpha t + c & \gamma \\ \gamma^* & \beta t + c' \end{pmatrix}, \quad (7)$$

the Landau-Zener tunnel probability is

$$T = \exp(-2\pi|\gamma|^2|\alpha - \beta|^{-1}). \quad (8)$$

The matrix (6) is of the form (7) in the basis where \mathcal{H}_1 is diagonal, so in that basis we can read off the coefficients α, β, γ needed to determine T .

For a specific example, we consider the Hamiltonian (1) with $v_{ij} = v_i\delta_{ij}$, which for $a_{\text{tilt}} > v_x$ represents a type-II Weyl cone. We find

$$T = \exp\left(-\frac{\pi\hbar v_x^2 E^2 + v_y^2 k_y^2 (a_{\text{tilt}}^2 - v_x^2)}{eB v_z (a_{\text{tilt}}^2 - v_x^2)^{3/2}}\right)$$

$$= \exp\left(-\frac{\pi\hbar}{4eBv_z} (\Delta k)^2 (a_{\text{tilt}}^2 - v_x^2)^{1/2}\right), \quad (9)$$

with Δk the minimal separation of the contours C_+ and C_- . (See Fig. 1.) This has the general form of the inter-band tunnel probability in the theory of magnetic breakdown [18, 22, 23], with a breakdown field $B_c \propto (\Delta k)^2$. The characteristic feature of Klein tunneling is that the tunnel probability $T \rightarrow 1$ and $B_c \rightarrow 0$ at the conical point of the band structure — here a 3D Weyl point and a 2D Dirac point in Ref. 13.

To illustrate the effect of Klein tunneling between electron and hole pockets on the magnetic quantum oscillations in the density of states, we consider the model

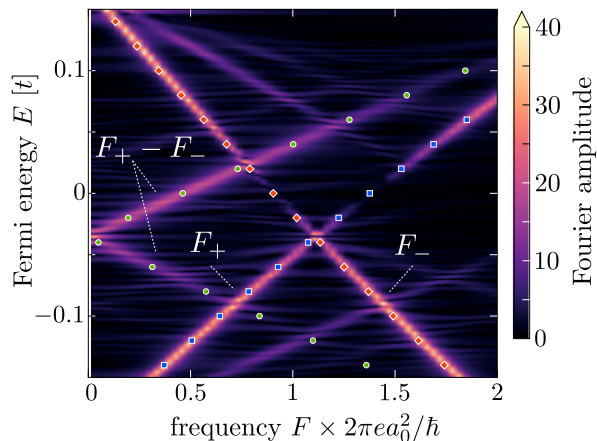


FIG. 3: Fourier amplitudes of the magnetic quantum oscillations. The numerical data for the partial density of states $\rho(E, k_y = 0)$ (smoothed with a Gaussian of width $\Gamma = t/500$) is Fourier transformed over the field range $B \lesssim 0.005 h/ea_0^2$ ($200 < N < 1500$). The fundamental frequencies for the electron and hole pockets are indicated by F_+ and F_- , respectively (the first harmonics are also faintly visible). Klein tunneling between the pockets when the Fermi energy approaches the Weyl point ($E = 0$) suppresses these high-frequency oscillations, introducing a new component at the difference frequency $|F_+ - F_-|$. The colored data points for F_{\pm} are the semiclassical prediction (4) from the extremal areas.

Hamiltonian [24]

$$\begin{aligned}
 H = & \tau_z(t'\sigma_x \sin k_x + t'\sigma_y \sin k_y) + t\tau_z\sigma_0 \sin k_z \\
 & + \tau_x\sigma_0(\mu - t \cos k_x - t \cos k_y - t \cos k_z) \\
 & + b\tau_0\sigma_z + [a_{\text{tilt}} \sin k_x + \xi(1 - \cos k_x)]\tau_0\sigma_0. \quad (10)
 \end{aligned}$$

This is a tight-binding Hamiltonian on a cubic lattice (lattice constant $a_0 = 1$), with a spin and orbital degree of freedom on each lattice site (Pauli matrices σ_i and τ_i , respectively). The time-reversal symmetry breaking term b splits the Dirac cone into two Weyl cones separated along the z -axis. To produce a type-II Weyl semimetal we have added a tilting term a_{tilt} and a term ξ that breaks the symmetry between the electron and hole pockets.

As derived in App. A, near a Weyl point the effective low-energy Hamiltonian has the form (1) with diagonal velocity tensor $v_{ij} = v_i\delta_{ij}$ given by

$$v_x = v_y = \frac{(2t - \mu)^2 - t^2 + b^2}{2b(2t - \mu)}t', \quad (11a)$$

$$v_z = \frac{1}{2b}\sqrt{[(t - \mu)^2 - b^2][b^2 - (3t - \mu)^2]}. \quad (11b)$$

The Hamiltonian (10) retains a mirror symmetry in the x - z plane (to be removed later on), which implies that for a magnetic field in the y -direction the areas $A_{\pm}(k_y)$ are extremal for $k_y = 0$. By means of exact diagonalization [26] we have calculated the partial density of states $\rho(E, B, k_y) = \sum_p \delta[E - E_p(B, k_y)]$ for $k_y = 0$, assuming that this gives the dominant contribution to

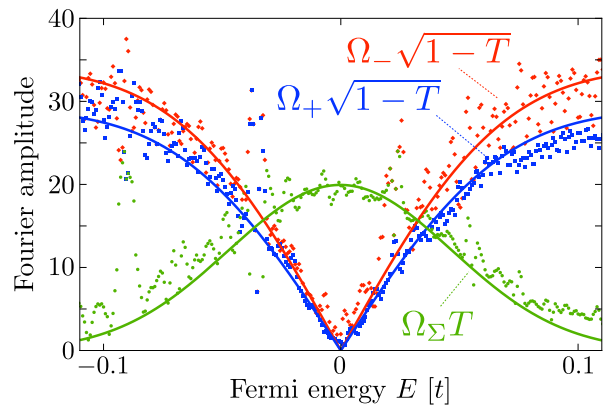


FIG. 4: Energy dependence of the Fourier amplitudes from Fig. 3. The curves are fits to $\Omega_{\pm}\sqrt{1-T}$ and $\Omega_{\Sigma}T$, with the transmission probability $T(E)$ calculated from Eq. (9) and energy-independent fit parameters $\Omega_{\pm}, \Omega_{\Sigma}$. When two frequency lines in Fig. 3 cross we cannot reliably determine the individual amplitudes — which explains some of the large scatter in the data points.

the magnetic quantum oscillations. We choose the gauge $\mathbf{A} = (0, 0, -Bx)$, with a rational flux $Ba_0^2 = 1/N \times h/e$ through a unit cell. The lattice has dimensions $N \times NM$ in the x - z plane ($M \gg N \gg 1$), with periodic boundary conditions in both directions.

Fig. 2 shows the energy spectrum as a function of magnetic field and Fig. 3 shows the periodicity of the magnetic oscillations, extracted from a Fourier transform of the density of states. When the Fermi level is far from the Weyl point $E = 0$, the electron and hole pockets contribute separately with frequencies F_{\pm} set by the extremal areas \mathcal{A}_{\pm} . The slopes dF_{\pm}/dE have opposite sign in the two pockets, signifying the opposite sign of the cyclotron effective mass

$$m_{\pm} = \frac{\hbar^2}{2\pi} \frac{d}{dE} |\mathcal{A}_{\pm}|. \quad (12)$$

Near the Weyl point a low-frequency component appears at the difference $|F_+ - F_-|$, and the individual high-frequency components F_{\pm} are suppressed. In a semiclassical description, the orbit responsible for the difference frequency is the “figure of eight” orbit formed by joining C_+ to C_- at the Weyl point (see Fig. 1b). The corresponding effective mass

$$m_{\Sigma} = \frac{\hbar^2}{2\pi} \frac{d}{dE} |\mathcal{A}_+ + \mathcal{A}_-| \quad (13)$$

governs the Landau fan in Fig. 2,

$$E_p(B) = E_p(0) + p \times \hbar e B / m_{\Sigma}. \quad (14)$$

Notice the absence of a $1/2$ offset from the integer p , canceled by a Berry phase.

The tunnel probability (9) evaluates for our model parameters to $T(E) = \exp[-0.52 N(E/t)^2]$. In Fig. 4 we plot the peak heights of Fig. 3 as a function of energy.

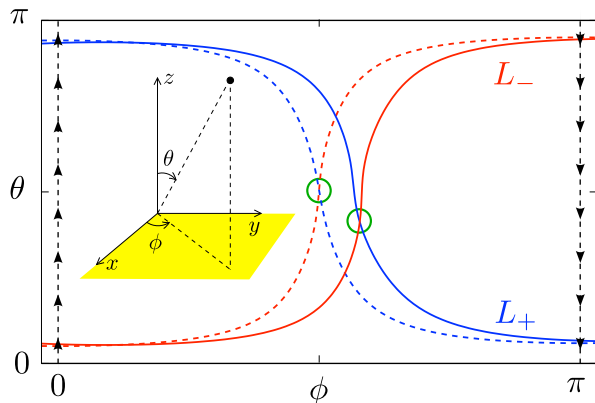


FIG. 5: Magnetic field axis $L_{\pm} = (\theta_{\pm}, \phi_{\pm})$ for which the extremal contour C_{\pm} at $E = 0$ touches the Weyl point. The dashed curves correspond to the Hamiltonian (10) with the parameters of Fig. 1. For the solid curves we have broken the mirror symmetry by adding the term $V_0\tau_0\sigma_0\sin k_y$ with $V_0 = 0.5$. The intersection of L_+ and L_- (encircled) is the special axis at which Klein tunneling between electron and hole pockets produces magnetic quantum oscillations with the difference frequency $|F_+ - F_-|$, suppressing both the electron and hole frequencies F_{\pm} . The intersection is protected by the topology of the Möbius strip (indicated by arrows, which show how the edges at $\phi = 0, \pi$ should be glued with a twist).

The solid lines are fits to $\Omega_{\pm}\sqrt{1-T(E)}$ and $\Omega_{\Sigma}T(E)$, with energy-independent fit parameters $\Omega_{\pm}, \Omega_{\Sigma}$. We take for the inverse field strength $N = 850$, half-way the interval used in the Fourier transform. A good match to the predicted Gaussian $T(E)$ is obtained.

The above analysis was simplified by the mirror symmetry in the x - z plane, because we could immediately identify the special magnetic field axis for which the extremal contours C_{\pm} in the electron and hole pockets both touch the Weyl point when $E \rightarrow 0$, allowing for Klein tunneling. One might wonder how restrictive this alignment is — is it possible to find such a special axis in

the absence of any symmetry? The answer is yes, as we demonstrate with the help of Fig. 5. At $E = 0$ we plot the polar and azimuthal angles θ_{\pm}, ϕ_{\pm} of the magnetic field axis for which the extremal contour C_{\pm} touches the Weyl point. Because (θ, ϕ) and $(\pi - \theta, \pi + \phi)$ represent the same axis, we may restrict ϕ to the range $[0, \pi]$ — half the usual range for spherical coordinates — identifying the end points $(\theta, 0)$ and $(\pi - \theta, \pi)$. The (θ, ϕ) plane with these “twisted” periodic boundary conditions is the so-called projective plane \mathbb{P}_2 , and has the topology of a Möbius strip.

If the loops $L_+ = (\theta_+, \phi_+)$ and $L_- = (\theta_-, \phi_-)$ both wind around the Möbius strip, as they do in Fig. 5, they must necessarily intersect because of the twist. The point of intersection is the special axis at which both C_+ and C_- touch the Weyl point. In App. B we show that such non-contractible loops always exist if the Fermi surface is convex, independent of any symmetry requirement.

Experimentally, Klein tunneling through a type-II Weyl point can be detected in measurements of the De Haas-Van Alphen effect in the magnetic susceptibility: If the magnetic axis is rotated towards the special alignment of Fig. 5, the high-frequency magnetic quantum oscillations from the electron and hole pockets would both be suppressed in favor of a low-frequency oscillation from the coupled orbits. The characteristic field for this magnetic breakdown would depend quadratically on the energy mismatch E between the Weyl point and the Fermi energy, with unit tunnel probability in the limit $E \rightarrow 0$ as the defining signature of Klein tunneling in momentum space.

The authors would like to thank I. Adagideli, P. Baireuther, J. A. Hutasoit, B. Tarasinski, and M. Wimmer for valuable discussions. This research was supported by the Foundation for Fundamental Research on Matter (FOM), the Netherlands Organization for Scientific Research (NWO/OCW), and an ERC Synergy Grant.

-
- [1] H. Weyl, *Z. Phys.* **56**, 330 (1929).
 - [2] C. Herring, *Phys. Rev.* **52**, 365 (1937).
 - [3] G. E. Volovik, *The Universe in a Helium Droplet* (Oxford University Press, 2003).
 - [4] T. Kawarabayashi, Y. Hatsugai, T. Morimoto, and H. Aoki, *Int. J. Mod. Phys. Conf. Series* **11**, 145 (2012).
 - [5] M. Trescher, B. Sbierski, P. W. Brouwer, and E. J. Bergholtz, *Phys. Rev. B* **91**, 115135 (2015).
 - [6] A. A. Soluyanov, D. Gresch, Z. Wang, Q.-S. Wu, M. Troyer, X. Dai, and B. A. Bernevig, *Nature* **527**, 495 (2015).
 - [7] G. Autés, D. Gresch, A. A. Soluyanov, M. Troyer, and O. V. Yazyev, arXiv:1603.04624.
 - [8] K. Koepnick, D. Kasinathan, D. V. Efremov, S. Khim, S. Borisenko, B. Büchner, and J. van den Brink, arXiv:1603.04323.
 - [9] M.O. Goerbig, J.-N. Fuchs, G. Montambaux, F. Piechon, *Phys. Rev. B* **78**, 045415 (2008).
 - [10] L. Huang, T. M. McCormick, M. Ochi, Z. Zhao, M. Suzuki, R. Arita, Y. Wu, D. Mou, H. Cao, J. Yan, N. Trivedi, and A. Kaminski, arXiv:1603.06482.
 - [11] S.-Y. Xu, N. Alidoust, G. Chang, H. Lu, B. Singh, I. Belopolski, D. Sanchez, X. Zhang, G. Bian, H. Zheng, M.-A. Hsuanu, Y. Bian, S.-M. Huang, C.-H. Hsu, T.-R. Chang, H.-T. Jeng, A. Bansil, V. N. Strocov, H. Lin, S. Jia, and M. Z. Hasan, arXiv:1603.07318.
 - [12] K. Deng, G. Wan, P. Deng, K. Zhang, S. Ding, E. Wang, M. Yan, H. Huang, H. Zhang, Z. Xu, J. Denlinger, A. Fedorov, H. Yang, W. Duan, H. Yao, Y. Wu, S. Fan, H. Zhang, X. Chen, and S. Zhou, arXiv:1603.08508.
 - [13] N. Harrison and S. E. Sebastian, *Phys. Rev. B* **80**, 224512 (2009).
 - [14] M.-C. Chang and M.-F. Yang, *Phys. Rev. B* **92**, 205201 (2015).

- [15] A. A. Zyuzin and R. P. Tiwari, arXiv:1601.00890.
 [16] N. W. Ashcroft and N. D. Mermin, *Solid State Physics* (Cengage Learning, 2011).
 [17] L. Onsager, Phil. Mag. **43**, 1006 (1952).
 [18] D. Shoenberg, *Magnetic Oscillations in Metals* (Cambridge University Press, 1984).
 [19] C. W. J. Beenakker, Rev. Mod. Phys. **80**, 1337 (2008).
 [20] R. Nandkishore and L. Levitov, PNAS **108**, 14021 (2011).
 [21] L. D. Landau and E. M. Lifshitz, Course of Theoretical Physics, Vol. 3 (Elsevier, Oxford, 1977).
 [22] E. I. Blount, Phys. Rev. **126**, 1636 (1962).
 [23] S. Keppeler and R. Winkler, Phys. Rev. Lett. **88**, 046401 (2002).
 [24] M. M. Vazifeh and M. Franz, Phys. Rev. Lett. **111**, 027201 (2013). The Hamiltonian (10) differs from that in this reference by the addition of the a_{tilt} and ξ terms, and also in the replacement of $\tau_y \sigma_0 \sin k_z$ by $\tau_z \sigma_0 \sin k_z$. This last change was introduced to produce small electron and hole pockets that do not spread out over the entire Brillouin zone.
 [25] E. Brown, Phys. Rev. **133**, A1038 (1964).
 [26] To discretize the model Hamiltonian (10) we used the KWANT toolbox: C. W. Groth, M. Wimmer, A. R. Akhmerov, and X. Waintal, New J. Phys. **16**, 063065 (2014).

Appendix A: Low-energy limit of the four-band model Hamiltonian of a type-II Weyl semimetal

The dispersion along the k_z -axis (for $k_x = k_y = 0$) of the four-band Hamiltonian (10) is given by

$$E_{\pm}^{\text{high}} = \pm b \pm \sqrt{(2t - \mu)^2 + t^2 + 2t(2t - \mu) \cos k_z}, \quad (\text{A1})$$

$$E_{\pm}^{\text{low}} = \pm b \mp \sqrt{(2t - \mu)^2 + t^2 + 2t(2t - \mu) \cos k_z}. \quad (\text{A2})$$

For $\mu > 2t$ the two low-energy bands E_{\pm}^{low} form a pair of Weyl cones located at

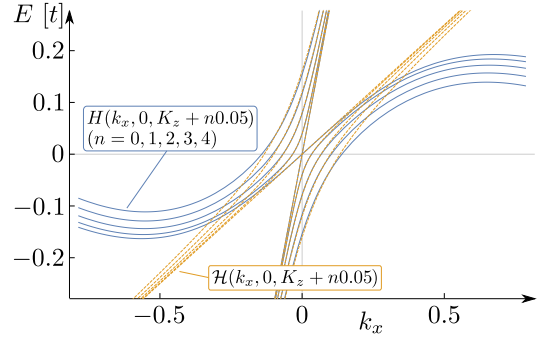


FIG. 6: Dispersion close to a type-II Weyl point. Shown are five k_z -subbands at $k_y = 0$; blue-solid lines show the dispersion of the four-band model (10); yellow-dashed lines show the corresponding low energy description (A8). Parameters are the same as in Fig. 2.

$$K_z = \pm \arccos \left(\frac{(2t - \mu)^2 + t^2 - b^2}{2t(\mu - 2t)} \right). \quad (\text{A3})$$

We wish to derive the corresponding low-energy Hamiltonian. Notice that for $k_x = k_y = 0$ the Hamiltonian (10) commutes with σ_z and is thus block-diagonal. Each of the two blocks contains one low and one high energy band. At $\mathbf{K} = (0, 0, K_z)$ the corresponding low energy eigenstates are given by

$$\Psi_+^{\text{low}} = \frac{1}{N_+} \left(\frac{(2t - \mu)(2b - 2t\sqrt{1 - \cos^2 K_z})}{(2t - \mu)^2 - t^2 + b^2}, 1, 0, 0 \right), \quad (\text{A4})$$

$$\Psi_-^{\text{low}} = \frac{1}{N_-} \left(0, 0, -\frac{(2t - \mu)(2b + 2t\sqrt{1 - \cos^2 K_z})}{(2t - \mu)^2 - t^2 + b^2}, 1 \right). \quad (\text{A5})$$

We expand the four-band Hamiltonian in the basis of these eigenstates:

$$\left(\begin{array}{cc|cc} \langle \Psi_+^{\text{low}} | H | \Psi_+^{\text{low}} \rangle & \langle \Psi_+^{\text{low}} | H | \Psi_-^{\text{low}} \rangle & \langle \Psi_+^{\text{low}} | H | \Psi_+^{\text{high}} \rangle & \langle \Psi_+^{\text{low}} | H | \Psi_-^{\text{high}} \rangle \\ \langle \Psi_-^{\text{low}} | H | \Psi_+^{\text{low}} \rangle & \langle \Psi_-^{\text{low}} | H | \Psi_-^{\text{low}} \rangle & \langle \Psi_-^{\text{low}} | H | \Psi_+^{\text{high}} \rangle & \langle \Psi_-^{\text{low}} | H | \Psi_-^{\text{high}} \rangle \\ \hline \langle \Psi_+^{\text{high}} | H | \Psi_+^{\text{low}} \rangle & \langle \Psi_+^{\text{high}} | H | \Psi_-^{\text{low}} \rangle & \langle \Psi_+^{\text{high}} | H | \Psi_+^{\text{high}} \rangle & \langle \Psi_+^{\text{high}} | H | \Psi_-^{\text{high}} \rangle \\ \langle \Psi_-^{\text{high}} | H | \Psi_+^{\text{low}} \rangle & \langle \Psi_-^{\text{high}} | H | \Psi_-^{\text{low}} \rangle & \langle \Psi_-^{\text{high}} | H | \Psi_+^{\text{high}} \rangle & \langle \Psi_-^{\text{high}} | H | \Psi_-^{\text{high}} \rangle \end{array} \right) = \left(\begin{array}{c|c} H_{\text{low}} & V_{\text{high,low}} \\ \hline V_{\text{high,low}}^\dagger & H_{\text{high}} \end{array} \right). \quad (\text{A6})$$

Note that at \mathbf{K} the high and low energy blocks are uncoupled ($V_{\text{high,low}}(0, 0, K_z) = 0$). Close to the Weyl point we have

$$\mathcal{H} \approx H_{\text{low}} + V_{\text{high,low}}^\dagger (H_{\text{high}})^{-1} V_{\text{high,low}}. \quad (\text{A7})$$

Thus, to linear order in the deviation from \mathbf{K} we can neglect this coupling and simply linearize H_{low} . After some algebra we find the corresponding low-energy Weyl

Hamiltonian,

$$\mathcal{H} = a_{\text{tilt}} k_x \tilde{\sigma}_0 - v_x k_x \tilde{\sigma}_x + v_y k_y \tilde{\sigma}_y + v_z (k_z - K_z) \tilde{\sigma}_z. \quad (\text{A8})$$

The matrices $\tilde{\sigma}_{0,x,y,z}$ are the identity and the Pauli matrices in the basis of $|\Psi_{\pm}^{\text{low}}\rangle$. The anisotropic velocity components were given in the main text, Eq. (11).

Fig. 6 shows a comparison between the type-II Weyl cone of the four-band model and its effective low-energy

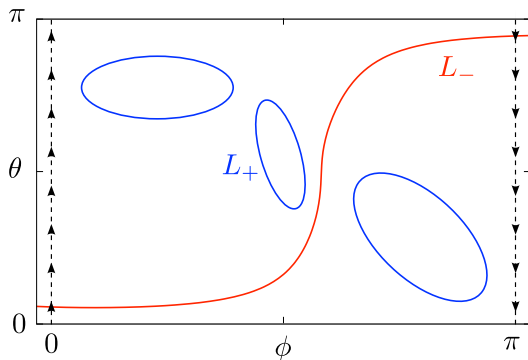


FIG. 7: Same as Fig. 5, but now the incontractible loop L_+ is replaced by a set of contractible loops, containing the entire set of magnetic field axes with extremal contours in the electron pocket that touch the Weyl point. This arrangement would avoid the topological protection of the intersection of incontractible loops in a Möbius strip, but we show by contradiction that it cannot happen in a convex electron pocket.

description.

Appendix B: Topological protection of the special magnetic field axis for Klein tunneling between electron and hole pockets

The topology of the Möbius strip (the projective plane \mathbb{P}_2) protects the intersection of two incontractible loops, ensuring the existence of a special magnetic field axis

where the extremal contours \mathcal{C}_\pm in the electron and hole pockets both touch the Weyl point at $E = 0$. This is the arrangement shown in Fig. 5. Contractible loops can avoid the intersection, as they do in Fig. 7. For convex electron and hole Fermi surfaces the existence of incontractible loops is guaranteed by the following argument.

Consider the full set \mathcal{S}_+ of magnetic field axes for which the extremal contour \mathcal{C}_+ in the electron pocket touches the Weyl point. If this set would consist only of contractible loops, then we would be able to pass an incontractible loop L through \mathbb{P}_2 that avoids \mathcal{S}_+ . We will now see that this leads to a contradiction.

For a convex Fermi surface each field axis \hat{n} on L is associated with a unique extremal contour $C(\hat{n})$. By construction, the contour $C(\hat{n})$ lies in a plane normal to \hat{n} . The direction \hat{n} defines whether the Weyl point lies above or below this plane. Inversion of the axis produces the same extremal contour and therefore the same normal plane, with “above” and “below” interchanged. As we follow the incontractible loop L from polar angle $\phi = 0$ to $\phi = \pi$, the field axis is inverted, so at some axis \hat{n}_0 on L the Weyl point must move from above to below the plane. As the plane’s motion is continuous, this can only happen if the Weyl point actually lies on $C(\hat{n}_0) \in L$. This would mean that $C(\hat{n}_0) \in \mathcal{S}_+$, which we had excluded by the construction of L .

The same argument can be applied to the hole pocket, and we conclude that for both the (convex) electron and hole pockets there must exist incontractible loops L_\pm of field axes with extremal contours that touch the Weyl point.